ACS APPLIED MATERIALS & INTERFACES

Letter

www.acsami.org

Carbon Segregation-Induced Highly Metallic Ni Nanoparticles for Electrocatalytic Oxidation of Hydrazine in Alkaline Media

Tae-Yeol Jeon,[†,‡,§] Masahiro Watanabe,[⊥] and Kenji Miyatake*[,†,‡,⊥]

[†]Clean Energy Research Center and [⊥]Fuel Cell Nanomaterials Center, University of Yamanashi, 4 Takeda, Kofu 400-8510, Japan
[‡]JST CREST, 4-1-8 Honcho, Kawaguchi, Saitama 332-0012, Japan

Supporting Information

ABSTRACT: The important roles of Ni in electrocatalytic reactions such as hydrazine oxidation are limited largely by high oxidation states because of its intrinsically high oxophilicity. Here, we report the synthesis and properties of highly metallic Ni nanoparticles (NPs) on carbon black supports. We discovered that the heat treatment of as-prepared Ni NPs with an average particle size of 5.8 nm produced highly metallic Ni NPs covered with thin carbon shells, with negligible particle coarsening. The carbon shells were formed by the segregation of carbons in the Ni lattice to the surface of the Ni NPs, leaving highly metallic Ni NPs. X-ray photoelectron spectroscopic analyses revealed that the atomic ratio of metallic Ni increased from 19.2 to 71.7% as a result of the heat treatment. The NPs exhibited higher electrocatalytic activities toward the hydrazine oxidation reaction in alkaline solution, as compared to those of the as-prepared Ni NPs and commercial Ni powders.

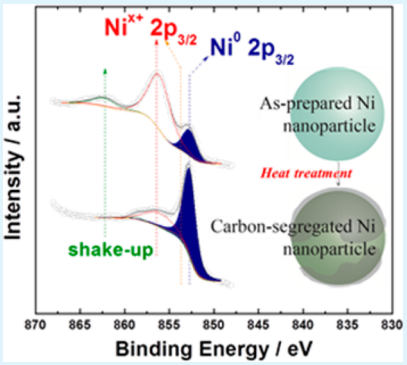

KEYWORDS: *carbon segregation, nickel nanoparticle, hydrazine oxidation, electrocatalyst*

The late first-row (3d) transition metal nanoparticles have long attracted scientific and technological interest because of their applications in various devices for energy conversion and magnetic storage.[1−5] These metal nanoparticles have a huge potential as electrocatalysts in alkaline media for the O_2 and CO_2 reduction reactions.[6,7] It has been recently reported that these non-noble metals, specifically, Ni and Co and their alloys, catalyze the electrochemical (faradaic) oxidation reaction of hydrazine to nitrogen and water via a four-electron transfer process, whereas noble metals such as Pt catalyze a chemical (nonfaradaic) reaction (decomposition) of hydrazine to nitrogen and hydrogen.[6] On the basis of this finding, various Ni-based binary and ternary alloy systems have been investigated for hydrazine oxidation reaction by using an electrochemical combinatorial array.[8−10] These previous reports focused on the effects of alloying rather than chemical states of 3d transition metal nanoparticles to enhance the electrocatalytic activity. Thus, dependence of the activity on chemical states in 3d transition metal nanoparticles has not been well studied, partly because of the lack of a facile synthetic route for highly metallic nanoparticles and their intrinsic susceptibility toward oxidation.[11−13]

A typical preparation method of preparing 3d transition metal nanoparticles such as Ni, Co, and Fe involves the decomposition of metal chelate complexes in the presence of strongly adsorbing stabilizers in the absence of oxygen-containing species such as air and water.[14−17] However, in most cases, the resulting nanoparticles are oxides rather than metals. Recently, it has been claimed that the thermal decomposition of Ni-oleylamine complexes with triphenylphosphine ($P(C_6H_5)_3$) could produce metallic Ni nanoparticles with nearly amorphous structure.[16] In this case, subsequent exposure to air caused rapid oxidation of the particles, resulting in the formation of NiO.

Metal nanoparticles are often anchored to carbon black supports with high surface area for applications as electrode materials such as fuel cell catalysts. The metal−carbon contact offers some advantages in stabilizing the nanoparticles against aggregation and enhancing catalytic activity.[18,19] There have not been many reports on the synthesis of late-3d transition metal nanoparticles dispersed on carbon black supports. It has been suggested that carbon supports could change the electron density of the 3d transition metal nanoparticles but not mitigate their surface oxidation under ambient conditions.[16,17]

Herein, we report a facile preparation method for highly metallic Ni nanoparticles on carbon black supports. We discovered that a carbon shell was formed in situ on the highly metallic Ni nanoparticles by surface segregation of a carbon-containing species (acetylacetonate $(C_5H_8O_2)_2$ in $Ni(acac)_2$ being the most probable source of the carbon), as a result of the heat treatment. The Ni nanoparticles supported on carbon black (Ni/CB) were found to show high catalytic activity toward hydrazine oxidation under alkaline conditions.

Ni/CB was prepared from $Ni(acac)_2$ by reduction with sodium borohydride ($NaBH_4$) in a solution containing 1,2-propanediol, oleylamine ($C_{18}H_{37}N$), and CB at 110 °C (see the

Received: August 29, 2014
Accepted: October 30, 2014
Published: October 30, 2014

Supporting Information for synthetic details). The reaction was carried out in the absence of oxygen-containing species (oxygen, water). Three samples with different Ni loading amounts (13.8, 22.0, and 28.7 wt % as nominal values) were prepared. The metal loadings of as-prepared Ni/CB (denoted as ASP-Ni) determined by elemental analysis were 12.3, 21.5, and 25.0 wt %, which corresponded to Ni recoveries of 88, 97, and 83% (see the Supporting Information). The ASP-Ni sample with 12.3 wt % Ni was heated at 400 °C for 4 h under a flow of a mixed gas of N_2 containing 5 vol % H_2 to remove organic moieties and to yield Ni nanoparticles with higher crystallinity (denoted as HT-Ni). Heat treatments were also performed under different atmospheres, i.e., pure N_2 and synthetic air (see the Supporting Information).

The structure of Ni/CB was analyzed by X-ray diffraction (XRD) (Figure 1a). The ASP-Ni sample did not show

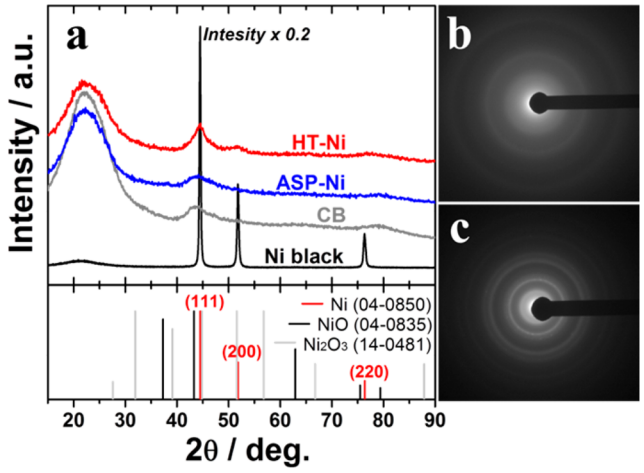

Figure 1. (a) Powder X-ray diffraction patterns of carbon black (CB), commercial Ni black, ASP-Ni (12.3 wt % Ni), and HT-Ni. Cu Kα radiation (50 kV, 200 mA). On the lower horizontal axis, red vertical lines represent the fcc Ni phase (JCPDS file 04−0850), black vertical lines the fcc NiO phase (JCPDS file 04−0835), and light gray lines the hexagonal closed-packed (hcp) Ni_2O_3 phase (JCPDS file 14−0481). The electron diffraction patterns of (b) ASP-Ni and (c) HT-Ni.

diffraction peaks assignable to Ni, NiO, or Ni_2O_3. Instead, it exhibited a weak, broad peak centered at 43.7°, which is very close to the (100) diffraction angle (43.5°) of graphitic carbon, as can be seen for the pattern for CB. In other words, its diffraction pattern is similar to that of carbon. The three ASP-Ni samples with different Ni-loadings (12.3, 21.5, and 25.0 wt %) showed similar XRD patterns (see Figure S2 in the Supporting Information). Its electron diffraction pattern (Figure 1b) also exhibited a bright center and diffuse rings, which are largely attributable to a carbon support, implying that the Ni of ASP-Ni was not crystalline. Compared to the ASP-Ni sample, the HT-Ni sample exhibited clear diffraction peaks centered at 44.5, 51.8, and 76.4° 2θ, which corresponded to the diffraction angles for (111), (200), and (220) of face-centered cubic (fcc) Ni (JCPDS file 04−0850), respectively. These peaks were also observed for commercial Ni black (see Experimental Methods). The HT-Ni sample did not exhibit peaks assignable to Ni oxides such as NiO or Ni_2O_3, whose diffraction patterns are shown on the lower horizontal axis of Figure 1a. The diffraction peaks of Ni are clearly seen, with several rings in the electron diffraction pattern (Figure 1c), which were indexed as (111), (200), (220), etc., from the center. These results suggest that crystalline Ni nanoparticles were formed after the heat treatment (HT-Ni). We dare not calculate the average particle size of the Ni nanoparticles using the Scherrer equation, because the Ni(111) peak was overlapped with the graphite (100) peak, and the Ni(220) peak was very low in intensity.

Images a and b in Figure 2 show TEM images of the ASP-Ni and HT-Ni samples. In both samples, the nanoparticles were

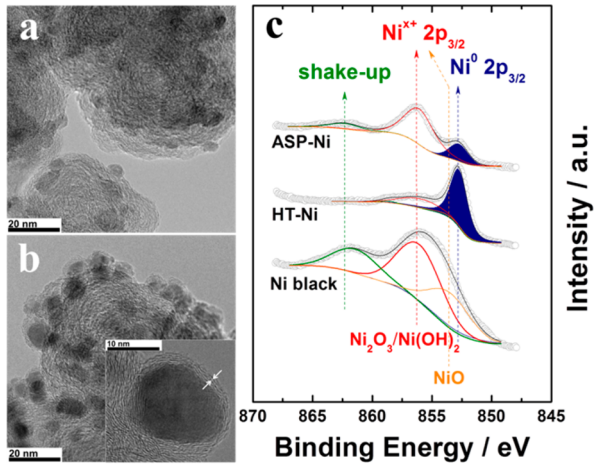

Figure 2. Transmission electron microscopic images of (a) ASP-Ni (12.3 wt % Ni) and (b) HT-Ni; (c) X-ray photoelectron spectra of the Ni $2p_{3/2}$ region for ASP-Ni, HT-Ni, and commercial Ni black.

highly dispersed on the carbon support. The mean particle diameters, which were determined by counting 100 randomly selected particles, were 5.6 ± 1.2 and 5.8 ± 1.5 nm for ASP-Ni and HT-Ni, respectively (see Figure S4 in the Supporting Information). Therefore, the heat treatment did not cause coarsening of the nanoparticles. Closer investigation of the HT-Ni sample in Figure 2b revealed that most Ni nanoparticles were covered by unidentified layers. The *d*-spacing of the layers seemed to be related to the plane-to-plane distance of graphite; the value was 0.38 ± 0.02 nm, which is very close to that of the hexagonal graphite (002) plane (0.34 nm) and is also comparable to that of the carbon support (0.39 ± 0.02 nm), as shown in the inset of Figure 2b. It has been reported that carburized Ni particles can segregate carbons to their surfaces and form carbon layers by heat treatement.[20−22] Therefore, it is reasonable to conclude that the shell consists mainly of carbon. These layers were also observed for the Ni nanoparticles heated under various conditions (see Figure S5 in the Supporting Information for pure N_2 and air).

It is considered in this study that the heat treatment caused the surface segregation of carbons and the concomitant formation of crystalline Ni nanoparticles. Therefore, it is worth investigating the source of the segregated carbon making up the carbon shell. 1,2-Propanediol as the solvent was an unlikely source of the carbon shell, since the reaction temperature at 110 °C was not high enough to cause decomposition of the solvent under the inert atmosphere. The most probable source was the acetylacetonate from $Ni(acac)_2$. To confirm this assumption, we prepared the Ni/CB sample from nickel chloride ($NiCl_2$) and heat-treated as a control experiment under the same conditions as mentioned above. The as-prepared Ni nanoparticles from $NiCl_2$ exhibited a similar XRD pattern to that of ASP-Ni (see Figure S8a in the Supporting Information). In contrast, the surface-covering

dx.doi.org/10.1021/am5058635 | ACS Appl. Mater. Interfaces 2014, 6, 18445−18449

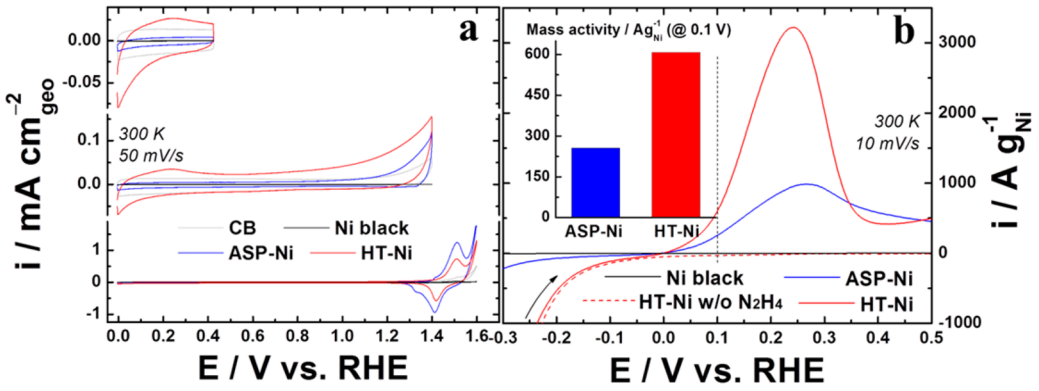

Figure 3. (a) Cyclic voltammograms for ASP-Ni, HT-Ni, CB, and commercial Ni black in 0.1 M NaOH (aq). The fifth scan for each catalyst is plotted. Current densities were normalized to the geometric area (0.283 cm^2) of the glassy carbon-disk electrode. The loading amount of Ni black on the glassy carbon electrode was equivalent to that of Ni nanoparticles in the Ni/CB samples. (b) Hydrodynamic voltammograms for ASP-Ni, HT-Ni, and commercial Ni black using a rotating disk (glassy carbon) electrode in 0.1 M N_2H_4 + 0.1 M NaOH (aq). The first scan for each catalyst is plotted (without prepotential cycling). The Ni black exhibited negligible current over the whole potential region examined. The voltammograms for the HT-Ni sample in the absence of hydrazine are also plotted for comparison (denoted by a dashed line). The rotation rate was 1600 rpm for all catalysts. The inset shows the $mass_{Ni}$-specific activities at 0.1 V. The amounts of Ni loaded on each electrode are based on the sample weight and the loading amount.

layers were not observed in the TEM images of the heat-treated sample (see Figure S8b in the Supporting Information). Similar results have been reported for Pd nanoparticles.[23,24] It was revealed that acetylacetonate from $Pd(acac)_2$ was a contaminant both in the bulk and on the surface of as-prepared Pd crystallites, and subsequent heat treatment induced surface segregation. Consequently, the Pd particles were partially or completely encapsulated by thin carbon layers. The previous reports[20−26] and our comparative studies of $Ni(acac)_2$ and $NiCl_2$ led us to conclude that acetylacetonate was the source of carbon present into the solid matrix.

Ni 2p core-level X-ray photoelectron spectra are shown in Figure 2c. The curve-fitting suggests that Ni exists in various states, such as 852.7 eV, corresponding to Ni^0, 853.5 eV (e.g., NiO) and 856.0 eV (e.g., Ni_2O_3 or $Ni(OH)_2$), corresponding to Ni^{x+}, respectively. The ratio among these states changed significantly as a result of the heat treatment. The atomic ratio of Ni^0 was calculated by subtracting the background from the spectrum and then performing a deconvolution, enabling the contribution of the Ni^0 peak to be separated from those of the other oxidation states, as well as from the shakeup satellite (ca. 862.3 eV). The atomic percentage of Ni^0 increased drastically, going from 19.2 to 71.7% after the heat treatment. The large increase in Ni^0 was also observed for the heat-treated samples under various atmospheres: in pure N_2 (62.7% Ni^0) and synthetic air (39.8% Ni^0) (see Figure S6 in the Supporting Information). The order of Ni^0 percentages decreased in the following order: N_2 + H_2 (5 vol %) > N_2 > air. The results are reasonable, taking into account the contributions of hydrogen gas in reducing oxidized Ni and those of oxygen gas in oxidizing metallic Ni at elevated temperatures. It should be noted that the segregation of carbon and the formation of a thin carbon layer took place for the heat treatment in all of these different atmospheres, whereas the content of metallic Ni was dependent on the presence of hydrogen or oxygen. Compared to the carbon-segregated Ni nanoparticles, the commercial Ni black contained only 2.7 at% of Ni^0. It is worthwhile to discuss the shakeup satellite peak at ca. 862.3 eV, which is often observed for Ni oxides such as NiO, $Ni(OH)_2$, and Ni_2O_3. It is well-known that the shakeup satellite is caused by the perturbation of the central potential upon photoionization of an inner shell electron, attributed to a valence electron excited by an emitted 2p photoelectron; this peak is not observed for metallic Ni with fcc structure.[27,28] In other words, the shakeup peaks are indicative of Ni oxides. The shakeup peak was observed for the ASP-Ni sample but exhibited a negligible contribution to that for the HT-Ni sample. This result is consistent with the Ni 2p core-level spectra mentioned above and the XRD data.

Assuming that Ni oxides exist only in the outer layers of the spherical nanoparticles (Ni^0 core covered with a Ni oxide shell), the amount of oxidized Ni was calculated. The thickness of the surface oxide layer was estimated using the average particle size and the atomic ratio of Ni^0 obtained by TEM and XPS, respectively. The HT-Ni sample had a 4.3 nm diameter Ni core with a 0.7 nm thick oxide shell, which were much lower than the average diameter of Ni core (5.8 nm) and the average thickness of NiO shell (1.6 nm) reported in the literature.[17] The 0.7 nm thick shell corresponded to 2.7 monolayers of Ni oxide, which consisted of 87.0 at% Ni_2O_3 and 13.0 at% NiO. The *d*-spacing values of hexagonal Ni_2O_3(0002) and fcc NiO(111) were used to estimate the number of the surface oxide layers. The Ni nanoparticles treated under different atmospheres in pure N_2 and synthetic air had 3.3 monolayers (0.91 nm thick oxide shell and 4.0 nm diameter Ni^0 core) and 4.8 monolayers (1.33 nm thick oxide shell and 3.1 nm diameter Ni^0 core) monolayers of Ni oxide, respectively. Although these calculations are based on several approximations, it can reasonably be assumed that the Ni oxides exist within ca. 3−5 monolayers on the surfaces of the heat-treated Ni nanoparticles.

HT-Ni nanoparticles covered with thin carbon shells were highly stable to oxidation. After exposure to air for a certain period of time, there were no changes observed in the level of metallicity of HT-Ni; the same XPS results were obtained for the sample left in the air for 2 months. Compared to typical Ni nanoparticles reported in the literature that experienced rapid oxidation when contacted with air,[16,17] HT-Ni nanoparticles covered with thin carbon shells were much more stable.

Figure 3a shows cyclic voltammograms (CVs) for the CB, ASP-Ni, HT-Ni, and Ni black samples measured in three different potential ranges (from −0.006 to 0.425, 1.4, and 1.6 V vs RHE, respectively) in 0.1 M NaOH. The oxidative

dx.doi.org/10.1021/am5058635 | ACS Appl. Mater. Interfaces 2014, 6, 18445−18449

desorption of hydrogen absorbed in the Ni lattice is thought to be mainly responsible for the anodic peak at around 0.24 V, and metallic Ni is continuously oxidized to β-Ni(OH)$_2$ over 0.108 V, NiO over 0.132 V, and β-NiOOH over ca. 1.37 V.[29] CB exhibited a typical CV in each potential region, i.e., a featureless double layer region and current for the oxidation of carbon at potentials over ca. 1.1 V. The hydrogen desorption from Ni at 0.24 V was not observed for the ASP-Ni sample, indicating a lack of hydrogen absorbability. The result is in accordance with the XPS data mentioned above, i.e., that the ASP-Ni sample contained only a small amount of metallic Ni. The double layer currents for ASP-Ni were smaller than those of CB, probably because the deposition of Ni nanoparticles lowered the surface area of exposed carbons available for OH^- adsorption. In the potential region in which the oxygen evolution reaction (OER) begins, around 1.55 V, ASP-Ni showed higher OER current than those on HT-Ni, presumably because of the absence of carbon shells that can hinder the OER on Ni and prevent the Ni atoms from undergoing oxidation and dissolution. HT-Ni exhibited typical CVs for metallic Ni, including hydrogen desorption on Ni at 0.24 V, oxidation from α/β-Ni(OH)$_2$ to β-NiOOH at ca. 1.41 V, and the OER at ca. 1.55 V. These peak positions were only slightly lower than those for bulk Ni reported in the literature.[29,30] It is noteworthy that HT-Ni showed higher current densities for hydrogen absorption/desorption and Ni oxidation, compared with those for ASP-Ni. Taking the XPS data mentioned above into account, it is considered that the higher ratio of Ni^0 resulted in higher amounts of hydrogen absorption and higher anodic currents in each potential region. The CVs on the commercial Ni black showed much lower currents in the whole potential region and no characteristic peaks of Ni because of the very low content of Ni^0.

We have then investigated the catalytic activities of the CB, ASP-Ni, HT-Ni, and Ni black samples for the hydrazine oxidation reaction under alkaline conditions (in 0.1 M NaOH containing 0.1 M N_2H_4), as shown in Figure 3b. The large anodic peak on the positive-going potential scan at ca. 0.245 V corresponds to the oxidation of hydrazine but appears to depend on either the desorption of absorbed hydrogen or the oxidation of Ni^0 to NiO_x and α-Ni(OH)$_2$. The anodic currents between 0 and 0.1 V are considered to originate from the electrocatalytic reaction of hydrazine on Ni^0, because Ni^0 is thermodynamically stable in the potential range of −0.095−0.108 V. While both hydrazine and hydrogen oxidation reactions could contribute to the oxidation currents at 0.1 V,[6,29] the possibility of the latter reaction was ruled out by the control experiment; HT-Ni exhibited negligible anodic current in the absence of hydrazine. The mass$_{Ni}$-specific activity of HT-Ni at 0.1 V vs RHE was calculated to be 608 A/g, which was 2.4 times higher than that of ASP-Ni (256 A/g) (inset of Figure 3b). Ni black showed essentially no catalytic activity for the hydrazine oxidation reaction. These results, combined with the XPS data mentioned above, indicate that the content of metallic Ni plays a decisive role in the catalytic activities for the hydrazine oxidation reaction. Interestingly, the thin carbon shell was effective in protecting the metallic Ni from further oxidation in air, whereas it did not deactivate the catalytic activity of the Ni for hydrazine oxidation.

In summary, we have developed a new preparation method for highly metallic Ni nanoparticles supported on CB. Ni nanoparticles (ASP-Ni) with an average particle size of 5.8 nm were obtained by the chemical reduction of Ni(acac)$_2$ in the presence of oleylamine and 1,2-propanediol. Heat treatment of the ASP-Ni caused the formation of highly metallic Ni nanoparticles covered with thin carbon shells without particle coarsening. By combining TEM, XRD, and XPS analyses, it was concluded that carbon was present in the solid matrix and was segregated from the solid as a result of the heat treatment, leaving highly metallic Ni nanoparticles. The highly metallic Ni nanoparticles exhibited superior catalytic activity for the hydrazine oxidation reaction, with 2.4 times higher mass$_{Ni}$-specific activity than that of ASP-Ni. This new synthetic approach should also be applicable to the other 3d transition metals as electrocatalysts for a variety of electrochemical reactions, including the hydrazine oxidation, hydrogen oxidation, and oxygen reduction reactions. Because the carbon material used in this study (Ketjen black) contains amorphous components, applicability of this method to other carbon materials such as graphene and carbon nanotubes needs to be investigated.

■ ASSOCIATED CONTENT

Supporting Information

Experimental details, physical characterization, and electrode preparation. This material is available free of charge via the Internet at http://pubs.acs.org.

■ AUTHOR INFORMATION

Corresponding Author

*E-mail: miyatake@yamanashi.ac.jp.

Present Address

[§]T.-Y.J. is currently at Pohang Accelerator Laboratory, Pohang 790−784, Republic of Korea

Notes

The authors declare no competing financial interest.

■ ACKNOWLEDGMENTS

This work was partly supported by the Ministry of Education, Culture, Sports, Science and Technology (MEXT) Japan through a Grant-in-Aid for Scientific Research (26289254).

■ REFERENCES

(1) Wang, C.; Chi, M. F.; Li, D. G.; Strmcnik, D.; van der Vliet, D.; Wang, G. F.; Komanicky, V.; Chang, K. C.; Paulikas, A. P.; Tripkovic, D.; Pearson, J.; More, K. L.; Markovic, N. M.; Stamenkovic, V. R. Design and Synthesis of Bimetallic Electrocatalyst with Multilayered Pt-Skin Surfaces. *J. Am. Chem. Soc.* **2011**, *133*, 14396−14403.

(2) Sun, S. H.; Murray, C. B.; Weller, D.; Folks, L.; Moser, A. Monodisperse FePt Nanoparticles and Ferromagnetic FePt Nanocrystal Superlattices. *Science* **2000**, *287*, 1989−1992.

(3) Hyeon, T. Chemical Synthesis of Magnetic Nanoparticles. *Chem. Commun.* **2003**, 927−934.

(4) Elkins, K. E.; Vedantam, T. S.; Liu, J. P.; Zeng, H.; Sun, S. H.; Ding, Y.; Wang, Z. L. Ultrafine FePt Nanoparticles Prepared by the Chemical Reduction Method. *Nano Lett.* **2003**, *3*, 1647−1649.

(5) Hou, Y. L.; Kondoh, H.; Kogure, T.; Ohta, T. Preparation and Characterization of Monodisperse FePd Nanoparticles. *Chem. Mater.* **2004**, *16*, 5149−5152.

(6) Sanabria-Chinchilla, J.; Asazawa, K.; Sakamoto, T.; Yamada, K.; Tanaka, H.; Strasser, P. Noble Metal-Free Hydrazine Fuel Cell Catalysts: EPOC Effect in Competing Chemical and Electrochemical Reaction Pathways. *J. Am. Chem. Soc.* **2011**, *133*, 5425−5431.

(7) Reske, R.; Duca, M.; Oezaslan, M.; Schouten, K. J. P.; Koper, M. T. M.; Strasser, P. Controlling Catalytic Selectivities during CO_2 Electroreduction on Thin Cu Metal Overlayers. *J. Phys. Chem. Lett.* **2013**, *4*, 2410−2413.

(8) Sakamoto, T.; Asazawa, K.; Yamada, K.; Tanaka, H. Study of Pt-Free Anode Catalysts for Anion Exchange Membrane Fuel Cells. *Catal. Today* **2011**, *164*, 181−185.
(9) Sakamoto, T.; Asazawa, K.; Sanabria-Chinchilla, J.; Martinez, U.; Halevi, B.; Atanassov, P.; Strasser, P.; Tanaka, H. Combinatorial Discovery of Ni-Based Binary and Ternary Catalysts for Hydrazine Electrooxidation for Use in Anion Exchange Membrane Fuel Cells. *J. Power Sources* **2014**, *247*, 605−611.
(10) Yang, H.; Zhong, X.; Dong, Z.; Wang, J.; Jin, J.; Ma, J. A Highly Active Hydrazine Fuel Cell Catalyst Consisting of a Ni-Fe Nanoparticle Alloy Plated on Carbon Materials by Pulse Reversal. *RSC Adv.* **2012**, *2*, 5038−5040.
(11) Jeon, T. Y.; Yoo, S. J.; Cho, Y. H.; Lee, K. S.; Kang, S. H.; Sung, Y. E. Influence of Oxide on the Oxygen Reduction Reaction of Carbon-Supported Pt-Ni Alloy Nanoparticles. *J. Phys. Chem. C* **2009**, *113*, 19732−19739.
(12) Ghosh, T.; Leonard, B. M.; Zhou, Q.; DiSalvo, F. J. Pt Alloy and Intermetallic Phases with V, Cr, Mn, Ni, and Cu: Synthesis As Nanomaterials and Possible Applications As Fuel Cell Catalysts. *Chem. Mater.* **2010**, *22*, 2190−2202.
(13) Trotochaud, L.; Ranney, J. K.; Williams, K. N.; Boettcher, S. W. Solution-Cast Metal Oxide Thin Film Electrocatalysts for Oxygen Evolution. *J. Am. Chem. Soc.* **2012**, *134*, 17253−17261.
(14) Sapieszko, R. S.; Matijevic, E. Preparation of Well-Defined Colloidal Particles by Thermal Decomposition of Metal Chelates: I. Iron Oxides. *J. Colloid Interface Sci.* **1980**, *74*, 405−422.
(15) Sun, S. H.; Zeng, H. Size-Controlled Synthesis of Magnetite Nanoparticles. *J. Am. Chem. Soc.* **2002**, *124*, 8204−8205.
(16) Park, J.; Kang, E.; Son, S. U.; Park, H. M.; Lee, M. K.; Kim, J.; Kim, K. W.; Noh, H. J.; Park, J. H.; Bae, C. J.; Park, J. G.; Hyeon, T. Monodisperse Nanoparticles of Ni and NiO: Synthesis, Characterization, Self-Assembled Superlattices, and Catalytic Applications in the Suzuki Coupling Reaction. *Adv. Mater.* **2005**, *17*, 429−434.
(17) Railsback, J. G.; Johnston-Peck, A. C.; Wang, J. W.; Tracy, J. B. Size-Dependent Nanoscale Kirkendall Effect During the Oxidation of Nickel Nanoparticles. *ACS Nano* **2010**, *4*, 1913−1920.
(18) Ioannides, T.; Verykios, X. E. Charge Transfer in Metal Catalysts Supported on Doped TiO_2: A Theoretical Approach Based on Metal-Semiconductor Contact Theory. *J. Catal.* **1996**, *161*, 560−569.
(19) Ding, M. N.; Tang, Y. F.; Star, A. Understanding Interfaces in Metal-Graphitic Hybrid Nanostructures. *J. Phys. Chem. Lett.* **2013**, *4*, 147−160.
(20) Otsuka, K.; Abe, Y.; Kanai, N.; Kobayashi, Y.; Takenaka, S.; Tanabe, E. Synthesis of Carbon Nanotubes on Ni/Carbon-Fiber Catalysts under Mild Conditions. *Carbon* **2004**, *42*, 727−736.
(21) Li, X. S.; Cai, W. W.; Colombo, L.; Ruoff, R. S. Evolution of Graphene Growth on Ni and Cu by Carbon Isotope Labeling. *Nano Lett.* **2009**, *9*, 4268−4272.
(22) Yoon, S. M.; Choi, W. M.; Baik, H.; Shin, H. J.; Song, I.; Kwon, M. S.; Bae, J. J.; Kim, H.; Lee, Y. H.; Choi, J. Y. Synthesis of Multilayer Graphene Balls by Carbon Segregation from Nickel Nanoparticles. *ACS Nano* **2012**, *6*, 6803−6811.
(23) Krishnankutty, N.; Li, J.; Vannice, M. A. The Effect of Pd Precursor and Pretreatment on the Adsorption and Absorption Behavior of Supported Pd Catalysts. *Appl. Catal., A* **1998**, *173*, 137−144.
(24) Jeon, T. Y.; Yoo, S. J.; Park, H. Y.; Kim, S. K.; Lim, S.; Peck, D.; Jung, D. H.; Sung, Y. E. Electrocatalytic Effects of Carbon Dissolution in Pd Nanoparticles. *Langmuir* **2012**, *28*, 3664−3670.
(25) Ziemecki, S. B.; Jones, G. A.; Swartzfager, D. G.; Harlow, R. L. Formation of Interstitial Pd-C Phase by Interaction of Ethylene, Acetylene, and Carbon Monoxide with Palladium. *J. Am. Chem. Soc.* **1985**, *107*, 4547−4548.
(26) Bowker, M.; Counsell, J.; El-Abiary, K.; Gilbert, L.; Morgan, C.; Nagarajan, S.; Gopinath, C. S. Carbon Dissolution and Segregation in Pd(110). *J. Phys. Chem. C* **2010**, *114*, 5060−5067.
(27) Matienzo, L. J.; Swartz, W. E., Jr.; Grim, S. O. X-ray Photoelectron Spectroscopy of Tetrahedral and Square Planar Nickel(II) Compounds. *Inorg. Nucl. Chem. Lett.* **1972**, *8*, 1085−1091.
(28) Matienzo, L. J.; Yin, L. I.; Grim, S. O.; Swartz, W. E., Jr. X-ray Photoelectron Spectroscopy of Nickel Compounds. *Inorg. Chem.* **1973**, *12*, 2762−2769.
(29) Hall, D. S.; Bock, C.; MacDougall, B. R. The Electrochemistry of Metallic Nickel: Oxides, Hydroxides, Hydrides and Alkaline Hydrogen Evolution. *J. Electrochem. Soc.* **2013**, *160*, F235−F243.
(30) Corrigan, D. A.; Bendert, R. M. Effect of Coprecipitated Metal Ions on the Electrochemistry of Nickel Hydroxide Thin Films: Cyclic Voltammetry in 1M KOH. *J. Electrochem. Soc.* **1989**, *136*, 723−728.